Supporting Information

Methanobactin transport machinery

Laura M. K. Dassama[a], Grace E. Kenney[a], Soo Y. Ro[a], Eliza L. Zielazinski[b], and Amy C. Rosenzweig[a,b,1]

[a]Departments of Molecular Biosciences and [b]Chemistry, Northwestern University, Evanston, IL 60208

Supporting Materials and Methods

Bioinformatics analysis. Genes in Mbn operons were identified as previously described (1). Homologues outside of Mbn operons were identified in the JGI-IMG database using PFAM or TIGRFAM hidden Markov models (HMMs) (PF07715 for TBDT plug domains, PF00593 for TBDT beta barrels, and PF00496 for family 5 of the bacterial extracellular solute (periplasmic) binding proteins). Predicted amino acid sequences and metadata (Files S1, S2) were obtained for genes of interest found in proteobacteria within the IMG database.

For phylogenetic analysis, genes of interest were aligned to the appropriate PFAM profile hidden Markov model using hmmalign (HMMER 3.1) (2). Truncated genes were manually removed, and additional domains were masked prior to phylogenetic analysis. All remaining domains were aligned using the L-INS-I mode of MAFFT. Approximate-maximum likelihood trees were inferred with FastTree 2.1.7 using the JTT+CAT model with branches rescaled using a Gamma20 likelihood, and were visualized using FigTree 1.4.0.

For clustering of genes, sequence similarity networks were generated as described in previously (3). Nodes represent the protein sequences for a given profile HMM, and edge values were generated via an all-by-all BLAST+ (NCBI) of those protein sequences against a database consisting of all the protein sequences, trimmed but un-aligned. Initial networks were generated using the Blast2Sim plug-in in Cytoscape 2.8.3 (4, 5) with an initial BLAST threshold of 100, a coverage factor of 15, and a "sum of all hits" similarity function. Low similarity values were used to cull edges according to a numeric filter; where appropriate, filter levels were adjusted until the partition of genes into groups reflecting native protein functionality was observed. Transitivity clustering was applied via the TransClust plugin. We used a starting threshold of 40

with the Blast2SimGraph_sim score as an edge value and similarity as an edge weight determiner. A tab-delimited text file identifying characteristics of interest for each node was loaded and overlaid onto the network via the Cytoscape VizMapper plug-in (4). Protein sequences associated with proteins of known function were used to provisionally categorize clusters or branches. Genus and gene length were obtained from exported JGI metadata for each gene, while phylum was determined using the NCBI Taxonomy Database on the basis of genus (http://www.ncbi.nlm.nih.gov/taxonomy).

Both protein families were investigated beyond the proteobacterial phylum using the EFI Enzyme Similarity Tool (6) to construct additional sequence similarity networks (Files S3, S4). Expectation value cutoffs were chosen as described previously (6); sequences with > 90% sequence identity were collapsed into a single node. Metadata were obtained from Uniprot or JGI/IMG, and clusters containing nodes corresponding to proteins with experimental support were identified.

Quantitative real-time PCR. RNA isolation, primer design and validation, cDNA synthesis, quantitative real-time PCR, and data analysis were performed as previously described (7). Briefly, RNA was isolated from copper starved *Ms. trichosporium* OB3b cells grown in spinner flasks before and at three timepoints (15 min, 5 h, 24 h) after the addition of 12.5 μM $CuSO_4$. At the point of harvesting, cells were added to a phenol/ethanol stop solution and processed using Qiazol in combination with an RNeasy midi kit, including an on-column DNase treatement (Qiagen). Additional gDNA contamination was removed using a Turbo DNAfree kit (Ambion). Initial quality control and quantification was performed on a Nanodrop 1000 (Thermo), but a Bioanalyzer (Agilent) was used for additional analysis (Table S3). cDNA was synthesized using

a SuperScript VILO kit using random hexamer primers and 1µg RNA template, following the manufacturer's instructions (Invitrogen).

qRT-PCR reactions were prepared using Express SYBR GreenER Universal 2x Master Mix (Invitrogen); 1.2 µL of RNase-free water containing 1ng of cDNA (or other amounts for primer efficiency trials), and 1.2 µL of 2x mastermix were added to each well in a white Bio-Rad 384-well plate using a Mosquito HTS liquid handling device (TTP). 96µL of primers (stocks of 5 µM each, forward and reverse) were added using an Echo liquid handler (Labcyte). Plates were sealed, centrifuged, and incubated for 1 h at 4 °C. qRT-PCR was performed in Bio-Rad CFX 384 thermocyclers, beginning with an initial 2 min UDG inactivation step at 50 ºC, followed by 2 min at 95 ºC. A total 40 amplification cycles were performed, with melting at 95 ºC for 15 s and annealing/extension at 60 ºC for 1 min, during which plate reading occurred. Following amplification, melt curves were obtained for each reaction by performing a plate reading step for 5 s from 50-90 ºC at 0.5 ºC intervals. Melt curves were analyzed and initial quality control were performed using CFX Manager (Bio-Rad), but most data analysis was performed using qbase+ (Biogazelle). Spearman correlation tests and one-way ANOVA tests were performed using qbase+. Hierarchical clustering of gene expression values was performed with Cluster 3.0 using complete linkage and either Spearman rank correlation or Euclidean distance as a similarity metric, and heatmap visualization of the clustered expression data was visualized using Java TreeView 1.1.6r4.

All primers used are listed in Table S4, along with experimentally determined primer efficiencies. Primers were designed as previously described (8) with 5 initial primers designed per gene in IDT PrimerQuest. Primer efficiency was assayed for each primer set using a seven point set of fourfold dilutions from 2 ng to 488 fg cDNA per reaction; all Cq values below 5 or

greater than 35 were discarded and efficiency was calculated in qbase+ (Biogazelle) (Table S4). Melt curves were performed for each reaction, and any primer set exhibiting evidence for two products was discarded. Primersets that only exhibited formation of primer dimers in the absence of template were maintained if no evidence for secondary amplicons or melt curve peaks was visible in the actual reactions, and all other primer alternatives performed more poorly. Amplicon sizes were confirmed using a 4% NuSieve 3:1 agarose (Lonza) gel in 1x TBE (Fig. S17). Acceptable sets of reference genes for these experiments were previously identified (7) (*alaS, glyA, pssA, ptsH, recA,* and *secA*); sequences and efficiencies are also available in Table S4. Statistical analysis (*vide infra*) is presented in Table S1 and File S5.

Gene-disruption mutant of *Ms. trichosporium* OB3b. The *Ms. trichosporium* OB3b Δ*mbnT* mutant was generated by removal of the *mbnT* gene through homologous recombination of a gene disrupting linear DNA fragment. The DNA fragment was produced by PCR amplification of the 5' and 3' DNA regions flanking the encoding gene and a gentamicin resistance gene (Table S5). The PCR products were joined together through assembly PCR in the order shown in Fig. S6. Wild type *Ms. trichosporium* OB3b cultures were grown in NMS medium with no copper, at 30 °C, and a gas mix containing a 1:3 methane-to-air ratio. 50 mL of cells were harvested at OD of 1.0, centrifuged at 7,000 × g, and washed with 10% sterile glycerol several times before a final 1 mL resuspension with 10% glycerol. The linear DNA fragment was introduced into *Ms. trichosporium* OB3b cells through electroporation. 100 μL of electrocompetent transformants were prepared using a Bio-Rad Gene Pulser at 2.2 kV and a 2 mm gap electroporation cuvette (Bio-Rad). The outgrowth cells were plated on NMS plates

containing gentamicin (10 μg/mL). The genotypes of the transformants were confirmed by PCR to detect the loss of 2 kb in the *mbnT* region of the genome (Fig. S6).

Growth conditions. *Ms. trichosporium* OB3b (wild type and mutant), *Mc. hirsuta* CSC1, *Mc. parvus* OBBP, and *Mc. rosea* SV97 were grown in NMS media without Cu as described previously (8) and harvested at late-exponential phase. Small cultures were grown in 250 mL flasks sealed with rubber septa at 30 °C and under a 1:3 methane to air gas ratio. Larger cultures were grown in 1 L spinner flasks (Chemglass) at 30 °C with stirring at 200 rpm and constant sparging with gas mix containing a 1:3 methane-to-air ratio. Gentamicin (2.5 μg/mL) was added to the cultures containing mutant strains.

CuMbn isolation and purification. Cells of WT *Ms. trichosporium* OB3b, *Mc. hirsuta* CSC1 or *Mc. parvus* OBBP were cultured as previously described (7), with the exception that no Cu was added to the growth media. Spinner flasks were treated with 5% nitric acid, followed by extensive washing with distilled, deionized water. Cultures producing apo Mbn (assessed by optical spectroscopy) were harvested by centrifugation. An excess of either natural abundance $CuSO_4$ or $^{65}CuSO_4$ was added to the spent medium, followed by filtration using a 0.2 μm filter. The filtered spent medium was loaded onto a Diaion HP-20 column (Sigma-Aldrich), and washed with 5-7 column volumes of 0.1 M potassium phosphate buffer pH 7.0. CuMbn was then eluted with a buffer containing 10 mM ammonium acetate (NH_4OAc) pH 6.0, and 60% HPLC-grade acetonitrile (ACN) or methanol (MeOH). CuMbn was detected by optical spectroscopy and MALDI or ESI mass spectrometry. CuMbn from *Mc. hirsuta* CSC1 was not further purified because of the low yield obtained after the Diaion HP-20 purification. To obtain fully purified

Ms. trichosporium OB3b and *Mc. parvus* OBBP CuMbn, Diaion HP-20 eluate fractions containing CuMbn were lyophilized, resuspended in water, and purified via reversed-phase HPLC on an Agilent 1000 HPLC using a 218TP54 analytical or 218TP1022 preparative C18 column (Grace Vydac). CuMbn was eluted over a gradient from 95% A (10 mM NH_4OAc)/5% B (80% ACN, 20% 10 mM NH_4OAc) to 45% A/55% B over 30 min at a flow rate of 1 mL/min or over 65 min at a flow rate of 5mL/min on the preparative column. The eluate was monitored with a diode array spectrometer using the full 200-800 nm UV-visible spectrum. Fractions were lyophilized and stored at - 20 °C.

^{65}CuMbn uptake assays. For uptake assays in *Ms. trichosporium* OB3b, WT and Δ*mbnT* cells were cultured until mid-log phase. The amount of cells present in each culture was estimated based on the optical density at 600 nm ($O.D._{600}$), and the volumes of cultures were adjusted (normalized) so that they were the same in all experiments. ^{65}CuMbn was added to aliquots of cultures to a final concentration of 5 μM. Cells were then incubated while shaking for 2 hr, and centrifuged at 18,000 × g for 5 min. The pellet was resuspended in 1 mL of a buffer containing 0.1 M potassium phosphate pH 7.0, 1 mM EDTA, and 0.05% Tween 80. The cells were centrifuged at 18,000 × g for 5 min, and resuspended twice in buffer containing 0.1 M potassium phosphate pH 7.0. After the final wash, the cells were resuspended in 100 μL of 67-70% nitric acid (trace metal grade) and heated at 95 °C for 1 hr to lyse the cells; ICP-MS samples were prepared after this step.

For uptake assays in *E. coli*, the pET-20b vector with and without the *mbnT* gene was chemically transformed into *E. coli* C41(DE3) and grown on LB-agar plates containing 100 μg/mL ampicillin sulfate. A single colony was grown in 5 mL of LB (also supplemented with

100 μg/mL ampicillin sulfate) for ~ 12 hrs at 37 °C. Then 1 mL of each culture was transferred to 50 mL of LB, grown at 37 °C to an $O.D._{600}$ of ~ 0.7. IPTG was added to a final concentration of 1 mM, and the cells were grown for an additional 3.5 hrs at 37 °C. At this point, the volumes of cultures were adjusted as described for uptake in *Ms. trichosporium* OB3b (*vide supra*) and centrifuged at 2500 × g for 5 min to pellet the cells. The cells were then resuspended in fresh media and ^{65}CuMbn was added to a final concentration of 5 μM. Samples were incubated while shaking at 37 °C for 30 min, centrifuged at 2,500 × g for 5 min, and resuspended in buffer containing 0.1 M potassium phosphate pH 7.0, 1 mM EDTA, and 0.05% Tween 80. Wash steps and ICP-MS sample preparation were carried out as described for *Ms. trichosporium* OB3b samples.

ICP-MS. All ICP-MS measurements were carried out at Northwestern University's Quantitative Bio-element Imaging Center on a Thermo iCap Qc ICP-MS. Multi-element standards (Inorganic Ventures, NWU-1) containing 0.1 – 200 ppb Cu were used to generate a standard curve for metal quantification. All samples and standards contained 3% nitric acid (trace metal grade, Sigma-Aldrich) and 5 ppb internal standard (multi-element IV-ICPMS-71D containing Bi, In, ^{6}Li, Sc, Tb, and Y; Inorganic Ventures). Three survey scans were performed during each run, and the average intensity was used to calculate the amount of metal isotope present.

Mass spectrometry. All MALDI-TOF mass spectrometry experiments were performed at Northwestern University's Integrated Molecular Structure Education and Research Center on an Autoflex III Smartbeam MALDI-TOF instrument (Bruker). The matrix was 20 mM *para*-nitroaniline (dissolved in 50% ethanol), and was added in a 1:1 (v/v) ratio to the sample being

investigated. All experiments were carried out in reflector instrument mode and negative ion mode with laser power less than 15%; m/z less than 500 Da and greater than 3000 Da were suppressed. The data were processed with Mnova (Mestrelab Research). All ESI mass spectrometry experiments were performed on an Amazon X ion trap mass spectrometer (Bruker) using electrospray injection. Samples were introduced via direct injection in a 50% MeOH/0.1% formic acid liquid phase and analyzed using both positive and negative ion modes; masses were acquired between 100 and 2000 Da.

Genomic DNA isolation and genome sequencing. Cultures to be used for genomic DNA isolation were grown as described in 1 L spinner flasks. Phenotypes were confirmed as previously described (7). Genomic DNA from pure cultures was purified using the MasterPure DNA isolation kit (Epicentre) followed by an additional RNase I digestion step (Epicentre), and cleanup of remaining enzyme using a Genomic DNA Clean and Concentrator kit (Zymo). DNA was quantified via Nanodrop (Thermo) and/or QuBit (Thermo).

For the *Mc. hirsuta* CSC1 genome sequencing, library production and sequencing were performed by ACGT Inc. The gDNA was used to prepare a 400–600 bp fragment multiplexed DNA library using a Nextera kit, and libraries were quantified using the KAPA Library Quantification Kit (Kapa Biosystems). Paired-end 2x150bp sequencing was performed on the sample using the Illumina MiSeq^{TM} platform. A total of 5,398,700 2x150bp reads were generated, with 400x coverage using *Methylocystis* sp. SC2 as a reference genome. Contigs containing operons of particular interest, including those containing the pMMO, sMMO, and Mbn operons, were extended manually via primer walking when necessary. The IGS Annotation Engine (9) was used for initial structural and functional annotation of the sequences (File S6),

with additional annotation upon upload to the JGI/IMG database. Manatee was used to view annotations (http://manatee.sourceforge.net/). Comparisons of the *Mc. hirsuta* CSC1 genome against other *Mc.* genomes were visualized using CGView (10).

Protein expression and purification. All primers are summarized in Table S6. To produce *Ms. trichosporium* OB3b MbnT, the region containing *mbnT* and ~ 500 base pairs up- and downstream was cloned from the genomic DNA of *Ms. trichosporium* OB3b. The full length *mbnT* was then cloned from this DNA with the insertion of restriction sites (HindIII and XhoI) and removal of the region coding for the first 19 amino acids using the following primers: forward, 5' GTCGACAAGCTTGCCGACTCGCCCGCAC-3' and reverse, 5'-GTGGTGCTCGAGGAATTCCACGCGAATG-3'. The PCR product was inserted into a pET-20b vector (Novagen), which encodes an N-terminal *pelB* leader peptide to direct export to the periplasm for outer membrane insertion, as well as a C-terminal hexa-histidine affinity tag. The presence of *mbnT* in the pET-20b vector was confirmed by sequencing (ACGT).

MbnT was expressed in Overexpress C41(DE3) cells (Lucigen). A single colony was cultured overnight in 100 mL of LB with 100 μg/mL ampicillin at 37 °C at 200 rpm. 10 mL of this culture was transferred to 1 L of LB; the larger cultures were grown to an $O.D._{600}$ of ~ 0.7. Protein expression was induced by the addition IPTG to 1 mM followed by incubation for 3.5 hrs. Cells were then harvested by centrifugation at 7,600 × g for 20 min, and resuspended in 25 mM Tris, 100 mM NaCl, pH 7.5 at a ratio of 1 g cell to 3 mL buffer. All purification steps were carried out at 4 °C to minimize thermal degradation of the protein. Prior to cell lysis, PMSF (dissolved in 95% ethanol) was added to the cells (1 μL/mL of a 250 mM stock solution) to prevent proteolysis. Cells were lysed via microfluidization, and PMSF was added as before. The

lysate was centrifuged at 8,000 × g at 4 °C for 30 min to pellet the cell debris. The supernatant from this step was centrifuged at 125, 000 × g for 1 hr to pellet all membranes. The pellet was resuspended in 25 mM Tris, 100 mM NaCl, pH 7.5 buffer using a Dounce homogenizer. Adding 2% N-lauroyl sarcosine (w/v) and stirring gently for 2 hrs selectively solubilized the inner membranes. The solution was centrifuged at 125,000 × g for 45 min to pellet the outer membranes containing MbnT. To solubilize the outer membranes, LDAO was added dropwise to a final concentration of 1% (w/v), and the solution was stirred gently for 1 hr. The solution was then centrifuged at 125,000 × g, and the supernatant was loaded onto Ni-NTA agarose resins. MbnT was purified via the batch method, and eluted with a buffer containing 300 mM imidazole. MbnT was concentrated and exchanged into buffer lacking imidazole and containing 0.5 % (w/v) LDAO. The protein purity was assessed via SDS-PAGE.

To clone MbnT from *Mc. rosea* SV97, the *mbnT* gene and ~ 500 flanking bases were cloned from the genomic DNA by PCR using the following primers: forward, 5' – TTTGCAGCACATTGCCGATG – 3'; reverse, 5' – TCGTTGCTGACATCTCCACG – 3'. To isolate the *mbnT* without a signal peptide and insert NcoI and XhoI restriction sites, another round of PCR with the following primers was carried out: forward, 5' – ACACGACCATGGCACAGCAGGCGCTTCCGC; reverse, 5' - TTCAGGCTCGAGAAACTT GAGTTTGATGCCTCCGG – 3'. The PCR product was double digested by NcoI and XhoI (NEB), cleaned up to remove enzymes (Qiagen), and ligated into a pET-20b vector encoding a C-terminal hexa-histidine affinity tag. The presence of *mbnT* in the vector was confirmed by sequencing. The protein was expressed in BL21(DE3) cells (Lucigen) using the protocol described for *Ms. trichosporium* OB3b MbnT.

The *mbnE* genes from *Ms. trichosporium* OB3b and *Mc. parvus* OBBP were cloned from their respective genomic DNA into the pSGC-His vector encoding a N-terminal hexa-histidine affinity tag by collaborators at the Albert Einstein College of Medicine; the *mbnE* from *Mc. hirsuta* CSC1 was cloned into the pET-20b vector, which encodes a C-terminal hexa-histidine affinity tag. N-terminal signal peptides were removed to ensure cytoplasmic expression. Starter cultures in the BL21(DE3) cell line (in LB media) were grown by shaking at 37 °C for 12 hr, followed by protein expression in ZYM-5052 autoinduction media (11). 1L cultures were grown at 37 °C until O.D.600 nm of 0.7-1.0; at this point, the temperature was changed to 18 °C for 12 hr. Cells were harvested by centrifugation as described for MbnT, and resuspended in buffer containing 25 mM Tris pH 7.5, 100 mM NaCl. Cells were lysed via microfluidization (2 passes through a chilled disruptor); PMSF (dissolved in ethanol) was added prior and after lysis, as described for the MbnT purification. All proteins were purified using the Ni-NTA agarose resin batch purification protocol and eluted with a buffer containing 300 mM imidazole. When necessary, additional rounds of purification were performed using size exclusion (120 mL Superdex 200 column, GE Healthcare) and/or anion exchange chromatography (60 mL HiLoad Q-sepharose column, GE Healthcare) using protocols recommended by the manufacturer.

Circular Dichroism (CD) spectroscopy. CD spectra were acquired on a Jasco J-815 spectropolarimeter at ambient temperature using 0.025 mg/mL and 0.05 mg/mL of *Ms. trichosporium* OB3b and *Mc. hirsuta* CSC1 MbnE, respectively, in a quartz cuvette with 2 mm path length. The spectral bandwith was 2 nm and 10 scans were accumulated for each protein. Spectra were deconvoluted using the DichroWeb server (http://dichroweb.cryst.bbk.ac.uk) using

the CONTINLL analysis program (12, 13) and reference sets SMP 180 (*Ms. trichosporium* OB3b MbnE) and Set 4 (*Mc. hirsuta* CSC1 MbnE) (Tables S7, S8).

SPR experiments and data analysis. All SPR experiments were performed on a Reichert SR7500DC Dual Channel System, using sensor chips also purchased from Reichert. All experiments with MbnTs were performed with a carboxymethyl dextran hydrogel surface sensor chip utilizing amine coupling with 1-ethyl-3-(3-dimethylaminopropyl)carbodiimide (EDC) and *N*-hydroxysuccinimide (NHS) to immobilize the protein. Prior to immobilization, the protein was exchanged into 25 mM MES buffer pH 6.5 to prevent EDC/NHS coupling with the primary amine in Tris buffer. The MbnEs were immobilized using the Nickel-Nitrilo Acid Sensor Chip. Continuous flow of buffer lacking detergent rendered MbnT samples effectively free of detergents. Substrates were applied in buffers without detergents. Data were first processed using the post-processing feature in the SPRAutolink software (Reichert Technologies) to generate file formats compatible with Scrubber (BioNavis), which permitted further processing to align and crop response curves, as well as to remove contributions from the reference channel. Processed data (text files) were plotted and fit using KaleidaGraph (Synergy Software).

Crystallization and structure determination of apo *Mc. parvus* OBBP MbnE. Purified MbnE was first crystallized in the MCSG sparse-matrix screens from Microlytic. In summary, 5 mg/mL protein was added in a 1:1 ratio with precipitant in sitting drop format at ambient temperature. Needle clusters appeared overnight and were optimized by streak seeding with lower concentrations of protein and precipitant. Ultimately, the best crystals were obtained with 3 mg/mL protein, and a precipitant solution of 0.1 M Bis-Tris pH 5.5, 0.2 M lithium sulfate, and

15% (w/v) PEG 3350. Crystals were soaked in a solution of 25% (w/v) PEG 400, 50% precipitant solution, and 25% water prior to freezing in liquid nitrogen. All data were acquired at the GM/CA-CAT beam line 23-ID-B at the Advanced Photon Source, Argonne National Laboratory. Data reduction was carried out with XDS (14, 15) (Table S2), and initial phases were obtained using Balbes (16) for molecular replacement with PDB 3PAM as a starting model. A model was built with Phenix AutoBuild (17), and multiple rounds of refinement and building were carried out in Coot (18) using REFMAC5 (19, 20) and Phenix Refine (17). Molprobity (21) was used to assess the quality of the model after each refinement cycle (Table S2). Figures were prepared using MacPyMOL2 (22).

Docking models of apo *Mc. parvus* OBBP MbnE with CuMbns. The server GRAMMX (http://vakser.compbio.ku.edu/resources/gramm/grammx/) was used to generate models of MbnE in complex with CuMbns from *Ms. trichosporium* OB3b (PDB 2XJH) and *Mc.* species strain M (PDB 2YGJ). The docking models generated contained only the unmodified peptide portion of CuMbn. To obtain a more accurate model, the docked MbnE structure was aligned with the full CuMbn structures. No significant change to the docked structures was observed upon alignment.

Supporting Results and Discussion

MbnT Bioinformatics. There are a number of differences between the different types of MbnTs. MbnT1s from Group I operons are found primarily in methanotrophic bacteria, ammonia-oxidizing bacteria, and cyanobacteria, and many alphaproteobacterial methanotrophs have multiple MbnT1s (Files S1-S3, Figs. S3*A*, *B*). These MbnT1s are not markedly similar to

any characterized TBDT groups using sequence-based phylogenetic or clustering analysis. MbnT2s from Group II operons are also found in methanotrophs and ammonia oxidizers along with a range of alphaproteobacterial species (although not cyanobacteria); many species have both MbnT1s and MbnT2s (Files S1-S3, Fig. S3*C*). MbnT2s are most similar to the uncharacterized *ycnD* TBDTs or Ni/Co transporters like NicT, but, like MbnT1s, are fully distinct from other characterized TBDT groups (Figs. S3*A*, *C*). Like MbnT2s, MbnT3s from Group III and IV operons lack the N-terminal extension and neighboring sigma/anti-sigma factor duo. However, unlike MbnT2s, MbnT3s are most similar to heme-transporting TBDTs such as *hasR* and *hemC* (Figs. S3*A*, *D*), and are not found in methane or ammonia oxidizers. They can be distinguished from heme-related TBDTs in part because genes encoding MbnT3s, like MbnT1s and MbnT2s, are frequently observed adjacent to genes encoding the uncharacterized proteins MbnP and MbnH, even when not in an Mbn operon.

Copper-regulated gene expression in the *mbn* operon and other genes of interest. qRT-PCR experiments were carried out in order to ascertain whether or not non-operon homologues of *mbnE* and *mbnT* are likely to play a significant role in the transport of the native *Ms. trichosporium* OB3b Mbn. We observed the copper-dependent regulation of genes of interest before and at three timepoints after addition of 12.5 μM $CuSO_4$ to copper-starved cells. Along with previously validated reference genes, we also analyzed the expression patterns of previously characterized copper-responsive genes for direct comparison against these new targets (*mbnE, mbnI, mbnT, mbnA,* and *mbnP* for the Mbn operon, *mmoR* and *mmoX* for the similarly copper down-regulated sMMO operon, and *pmoA* for the mildly copper up-regulated pMMO operon). For the two closest *mbnE* homologues, a hypothetical protein and a *yejA* homologue found

adjacent to genes encoding putative microcin C7 transport machinery, the answer is clear. Judged by any metric (Spearman correlation against *mbnE* (Table S1), one-way ANOVA (File S5), or hierarchical clustering of gene expression patterns (Fig. S5)), neither of these genes are co-regulated with *mbnE* and indeed neither display any statistically meaningful response to copper addition whatsoever.

Analysis of the two *mbnIRTPH* operons is more complex. First, regulatory genes and non-regulatory genes exhibit different behavior in the *mbn* operon: regulatory genes exhibit an immediate (0-15 min) response to copper addition, with almost all regulatory response occurring during that time period. This is true for one *mbnIRTPH* operon (containing *mbnT* MettrDRAFT_1229) but not the other (containing *mbnT* MettrDRAFT_1241), in which a slower response to Cu is observed (Fig. S5). Non-regulatory genes in the *mbn* operon are down-regulated primarily by the 5-24 h timepoints, and that is also observed for the *mbnIRTPH* operons (Fig. S5). However, the extent of Cu-stimulated down-regulation is less (particularly in *mbnPH*) and Spearman correlation values (Table S1) between these non-operon genes and select *mbn* operon genes (*mbnE, mbnI, mbnT, mbnA, mbnP*) are positive, but are markedly lower than within-operon correlations. Thus, these operons are clearly copper regulated, but they do not appear to be fully interchangeable with their counterparts in the *mbn* operon.

Finally, we also investigated *csp1*, a periplasmic "copper sponge" which was recently hypothesized (23) to interact with Mbn in the periplasm, a role that might reflect involvement in the Mbn transport pathway. However, our results support co-regulation with *pmoA* and *pmoB*, consistent with mild copper up-regulation and a primarily pMMO-related and not Mbn-related function.

Draft genome of *Mc. hirsuta* CSC1. Proteins from a range of methanotrophic species were investigated in this study. One of those species is *Mc. hirsuta* CSC1, for which there exists no published genome, but which is both commercially available and produces a previously characterized Mbn (24). To facilitate the use of proteins from this species, we sequenced its genome (File S6).

The contents of the *Mc. hirsuta* CSC1 draft genome (File S6) are consistent with its assignment as a member of the *Methylocystis* genus. Two *pmoCAB* operons corresponding to particulate methane monooxygenase (pMMO) are observed in the genome of this methanotroph, as are two monocistronic *pmoC* genes. No high methane affinity pMMO homologues (*pmoCAB2*) are present and neither are any *pxmABC* operons, unlike *Mc. parvus* OBBP and *Mc.* sp. SC2. Consistent with the phenotypic characterization of the type strain, genes encoding soluble methane monooxygenase (*mmoRGXYBZDC*) are present, but appear to be the result of horizontal gene transfer. A Group IIA methanobactin (Mbn) operon (*mbnETHPABCMFS*) is present, and the MbnA precursor peptide sequence (MTIRIAKRITLNVVGRAGAMCASTCAATNG) is consistent with the core peptide of the structurally characterized *Mc. hirsuta* CSC1 Mbn, and is highly similar to that of other Group IIA Mbn operons.

Genes encoding proteins related to the next steps of methane-derived carbon assimilation are also present. These include methanol dehydrogenase and related genes (*mxaFJGIRSACKL* as well as PQQ biosynthesis genes), enzymes involved in the tetrahydrofolate and tetrahydromethanopterin-related pathways (*ftr, fmd*, etc.) and formate dehydrogenase (*fdh*). Similarly, consistent with its status as a Type II methanotroph, genes encoding enzymes related to the serine cycle are also present.

Some genes related to nitrogen assimilation pathways are also present, including a *haoAB* operon, encoding hydroxylamine oxidoreductase, which enables this species to oxidize hydroxylamine to nitrite. Plasmid-borne nitrous oxide reductase genes present in *Mc.* sp. SC2 are not observed in this species. Other pathways of interest that are present include the ethylmalonyl-coenzyme A pathway for glyoxylate regeneration, enzymes involved in the TCA cycle and glycolysis, and enzymes involved in polyhydroxybutyrate production and metabolism. Comparison to other *Methylocystis* species (Fig. S18) indicates that *Mc. hirsuta* CSC1 is most closely related to *Mc.* sp. SC2, although some poorly conserved regions point towards the presence of probable genomic islands in that species.

Supporting Acknowledgements

qRT-PCR, SPR, ICP-MS, and mass spectrometry experiments were performed at the High Throughput Analysis Laboratory, the Keck Biophysics Facility, the Quantitative Bio-element Imaging Center, and the Integrated Molecular Structure Education and Research Center, all located at Northwestern University. X-ray crystallographic data were acquired at the GM/CA beam line 23-ID-B at the Advanced Photon Source (APS) at Argonne National Laboratory. GM/CA at APS has been funded in whole or in part with Federal funds from the National Cancer Institute (ACB-12002) and the National Institute of General Medical Sciences (AGM-12006). This research used resources of the Advanced Photon Source, a U.S. Department of Energy (DOE) Office of Science User Facility operated for the DOE Office of Science by Argonne National Laboratory under Contract No. DE-AC02-06CH11357. We thank the Institute for Genome Sciences Annotation Engine service at the University of Maryland School of Medicine for providing the initial annotation of the *Mc. hirsuta* CSC1 genome.

Supporting Figures

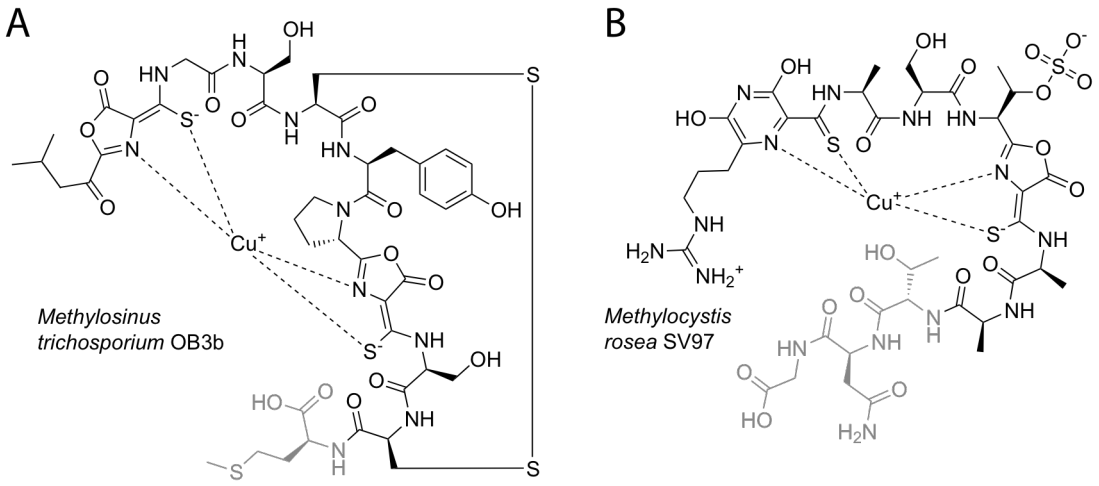

Fig. S1. Structures of CuMbns from *Ms*. *trichosporium* OB3b (*A*) and *Mc*. *rosea* SV97 (*B*). In both structures, two nitrogen-containing heterocycles and neighboring thioamide groups serve as ligands for a single copper ion. In *Ms. trichosporium* OB3b CuMbn, both heterocycles are oxazolones and two additional modifications (an N-terminal transamination and a disulfide bond) are present. In CuMbn from *Mc. rosea* SV97, the N-terminal oxazolone is replaced by a pyrazinedione, and although no disulfide bonds or N-terminal transamination modifications are apparent, a sulfonated threonine is present. Loss of some C-terminal residues (indicated in gray) is sometimes observed.

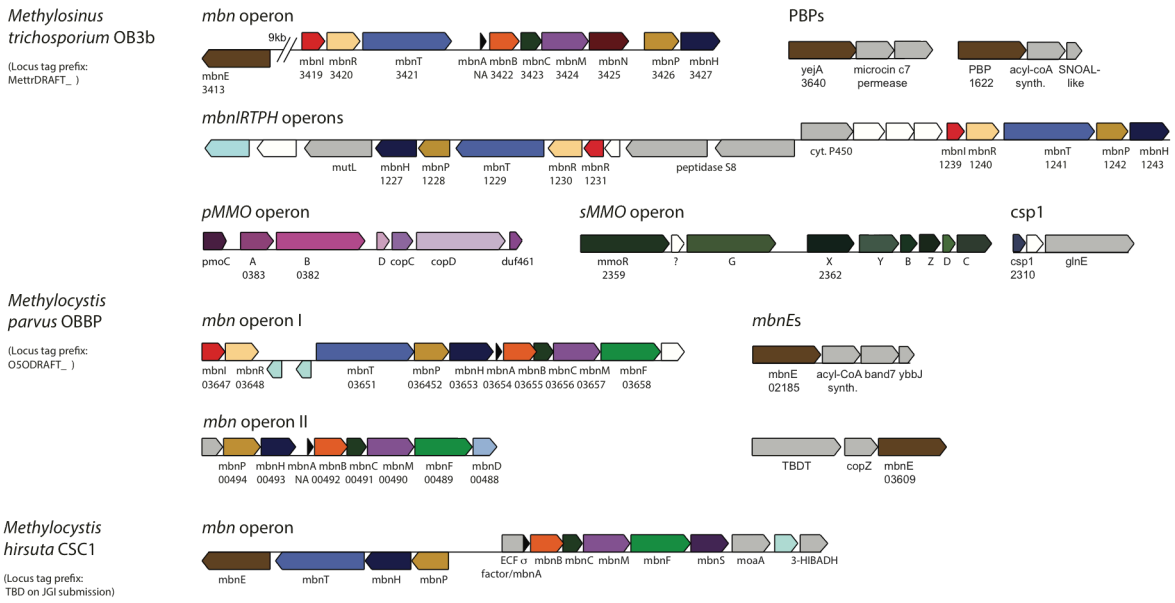

Fig. S2. Operons of interest, including both gene names and locus tags.

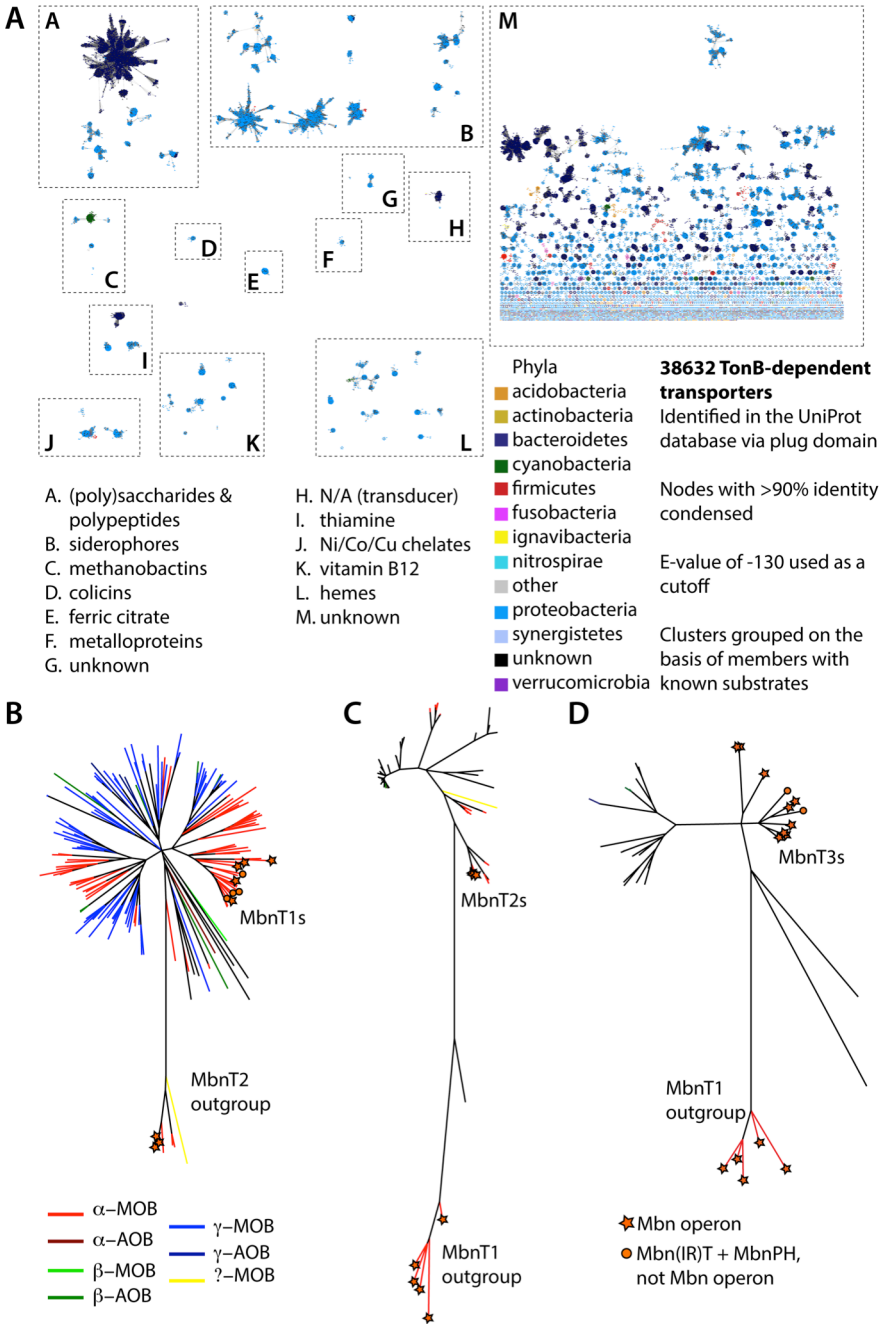

Fig. S3. (*A*) Sequence similarity network for 38682 TonB-dependent transporters, identified in UniProt. Only a minority of clusters contain transporters with known substrates; MbnTs clearly cluster independently of any characterized subgroups. (*B-D*) Full-length phylogenetic trees (generated in MEGA 5 using MAFFT-aligned sequences, maximum likelihood, WAG+F+G+1, and 1000 bootstrap rounds) for MbnT1s, MbnT2s, and MbnT3s respectively. Sequences were obtained from the IMG/JGI. The widespread nature of MbnT1s and, to a lesser extent, MbnT2s in methane oxidizing bacteria (MOB) and ammonia oxidizing bacteria (AOB) is clear; MbnT3s are generally found in non-methanotrophs.

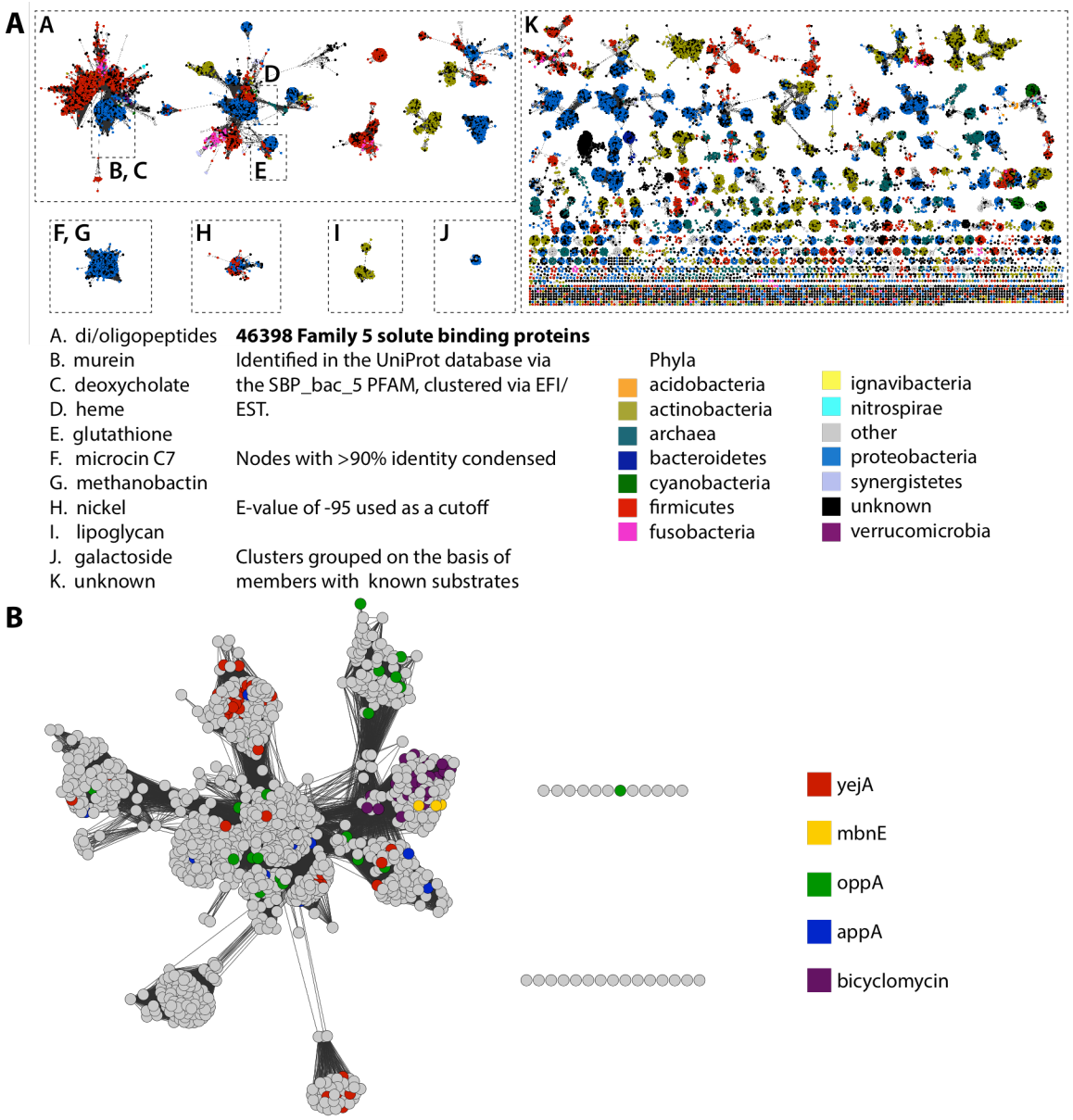

Fig. S4. (*A*) Sequence similarity network for all members of the periplasmic binding protein family 5 present in the JGI/IMG database. (*B*) Cluster containing *mbnE*, and *yejA* homologues, with nodes colored by annotated function and edges with an E-value worse than -151 deleted. "*OppA"* and "*appA*" are common annotations throughout SBP Family 5; annotations denoting a YejA homologue (a microcin C7 transporter), an MbnE homologue, or a bicyclomycin resistance protein appear to be unique to this subfamily.

A

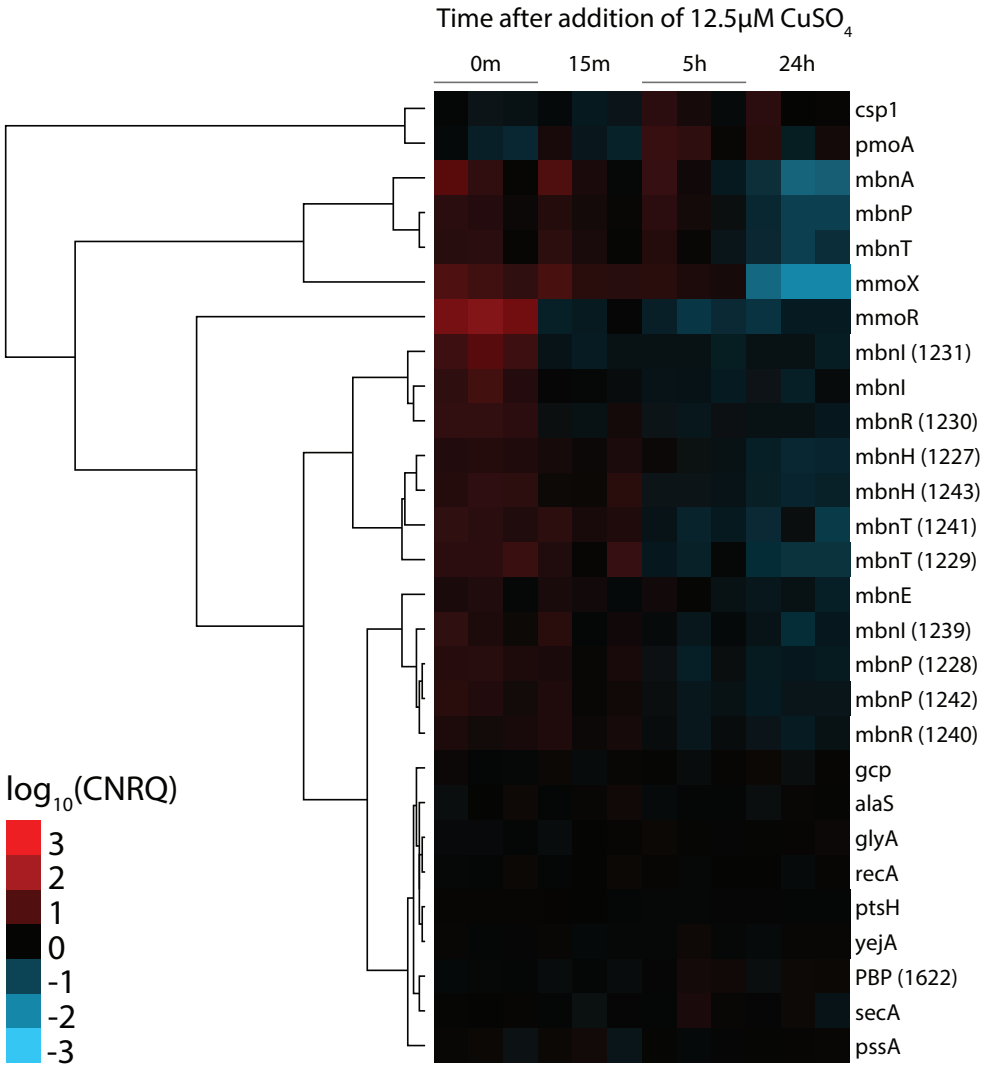
Time after addition of 12.5µM CuSO4
0m
15m
5h
24h
csp1
pmoA
mbnA
mbnP
mbnT
mmoX
mmoR
mbnI (1231)
mbnI
mbnR (1230)
mbnH (1227)
mbnH (1243)
mbnT (1241)
mbnT (1229)
mbnE
mbnI (1239)
mbnP (1228)
mbnP (1242)
mbnR (1240)
gcp
alaS
glyA
recA
ptsH
yejA
PBP (1622)
secA
pssA
log10(CNRQ)
3
2
1
0
-1
-2
-3

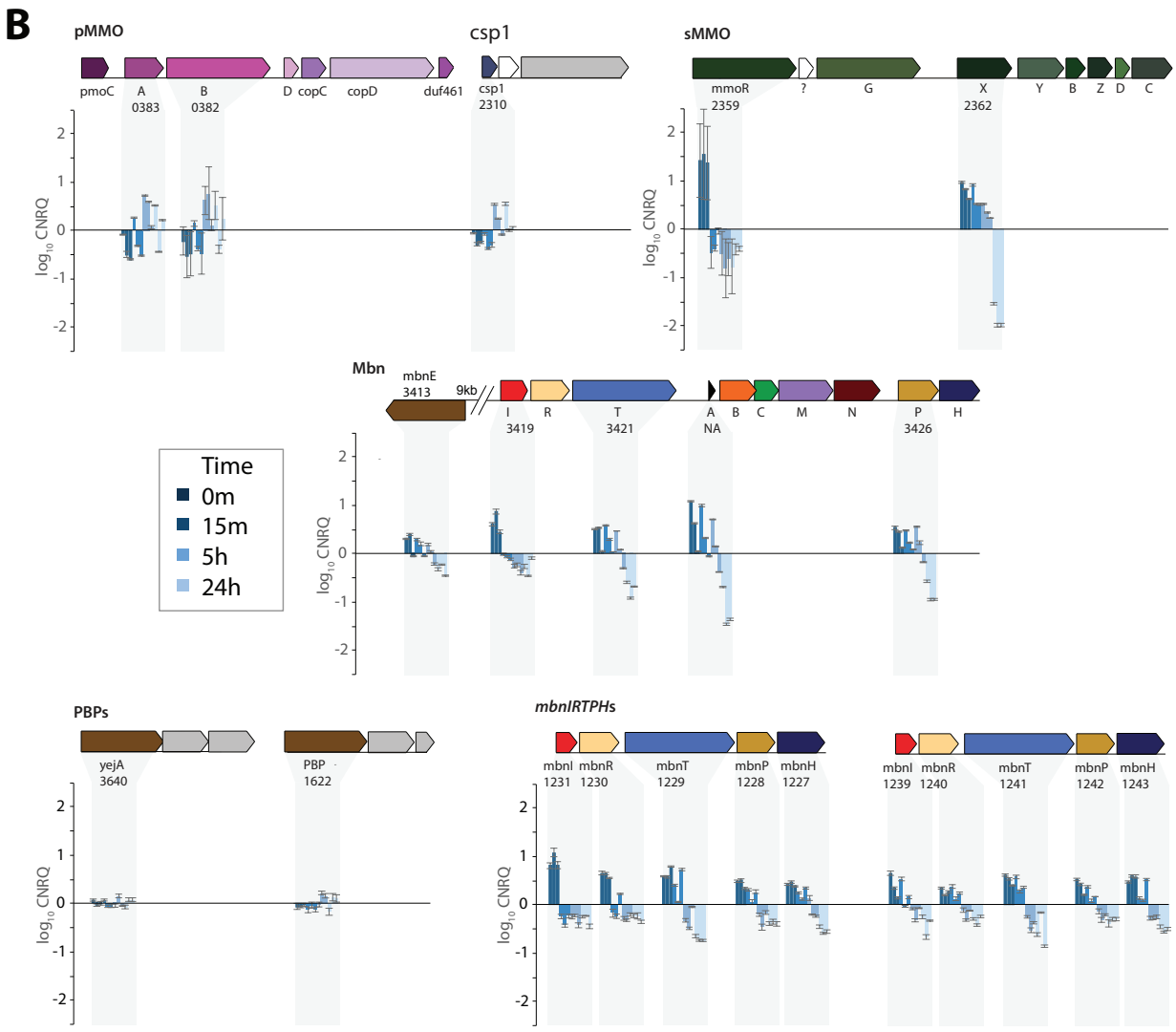

Fig. S5. qRT-PCR results. (*A*) Heatmap of gene expression levels at all four timepoints before and after copper addition, clustered by expression pattern. Members of the primary Mbn operon clearly exhibit expression patterns more similar to each other than to non-*mbn* operon homologues. As previously observed, regulatory genes cluster somewhat separately from the main *mbn* operon, except in the case of *mbnI3* and *mbnR3*, which do not show the swift (within 15 min) down-regulation seen in other regulators. Non-*mbn* operon PBPs exhibit minimal copper dependence. *Csp1*, which encodes a periplasmic copper binding protein suggested to interact with Mbn in vivo to facilitate copper transfer to pMMO, is co-regulated with genes belonging to the pMMO operon and not the *mbn* operon. (*B*) Bar graphs of qRT-PCR data. Error bars represent standard error.

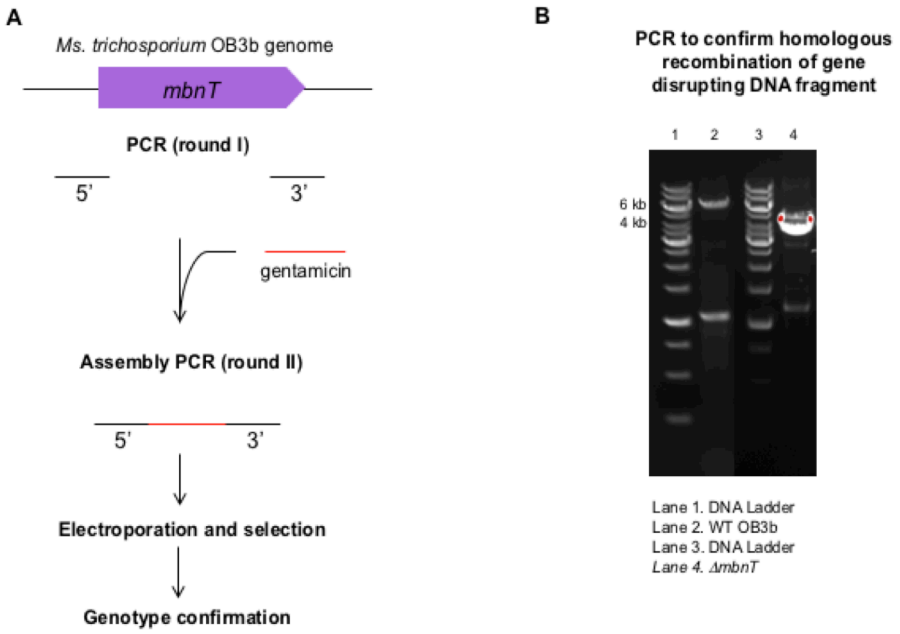

Fig. S6. Generation of the Δ*mbnT* gene disruption mutant of *Ms. trichosporium* OB3b. (*A*) Schematic depicting the fusion of DNA fragments by assembly PCR. (*B*) Agarose gel showing the loss of 2 kb band, corresponding to the loss of *mbnT*.

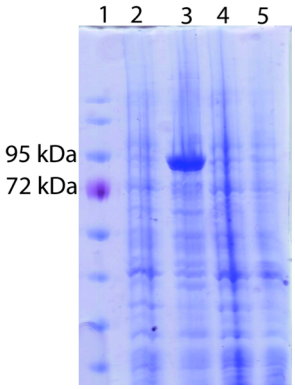

Fig. S7. SDS-PAGE gel showing the expression of *Ms. trichosporium* OB3b MbnT in *E. coli* C41(DE3) cells. Lane 1, PageRuler prestained molecular weight marker; lane 2, pET-20b_mbnT before IPTG addition; lane 3, pET-20b_mbnT after IPTG addition; lane 4, pET-20b before IPTG addition; lane 5, pET-20b after IPTG addition. The band at ~89 kDa in lane 3 corresponds to MbnT.

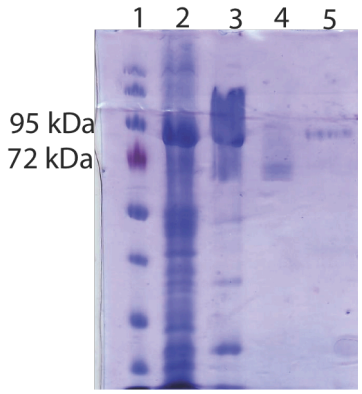

Fig. S8. SDS-PAGE gel showing purification of the *Ms. trichosporium* OB3b MbnT. Lane 1, PageRuler prestained molecular weight marker; lane 2, total membrane fractions; lane 3; isolated outer membrane fractions; lane 4, solubilized outer membrane fractions; lane 5, purified MbnT.

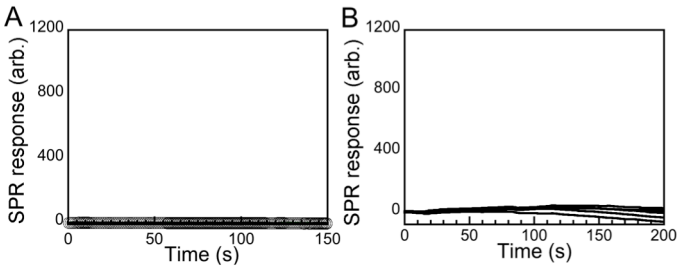

Fig. S9. SPR response curves showing application of (*A*) 4 μM each of cobalamin, ferric pyoverdine, and ferric citrate to *Ms. trichosporium* OB3b MbnT and (*B*) 1-16 μM CuMbn to myoglobin. The lack of appreciable SPR responses in these experiments suggests that the MbnT-CuMbn interaction is specific.

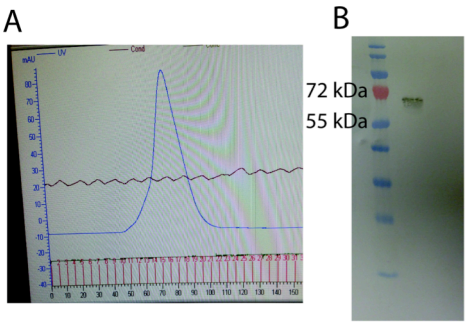

Fig. S10. Size-exclusion chromatogram (*A*) and Western blot (*B*) showing the purification of *Ms. trichosporium* OB3b MbnE. The 67.9 kDa protein elutes as a single oligomer from a Superdex 200 column.

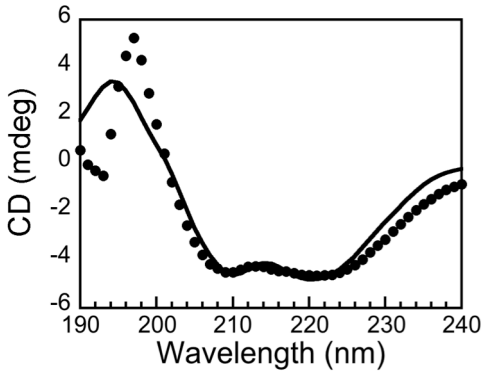

Fig. S11. CD spectrum and simulation thereof for the purified *Ms. trichosporium* OB3b MbnE. The spectrum was acquired as described in the text and simulated using parameters presented in Table S7.

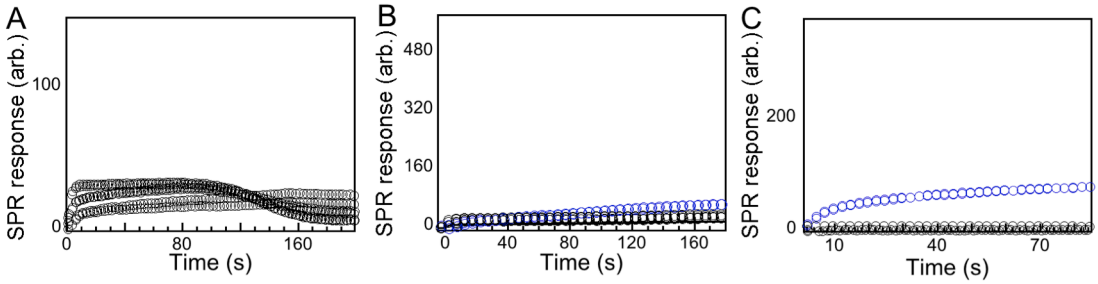

Fig. S12. SPR response curves of experiments investigating the substrate specificity of MbnEs. (*A*) *Ms. trichosporium* OB3b MbnE does not appear to bind 30 μM each of cobalamin, ferric pyoverdine, and $CuSO_4$. The MbnEs from *Mc. hirsuta* CSC1 (*B*) and *Mc. parvus* OBBP (*C*) do not bind 30 μM each of cobalamin, ferric pyoverdine, $CuSO_4$, and appreciable amounts of the CuMbn from *Ms. trichosporium* OB3b (blue).

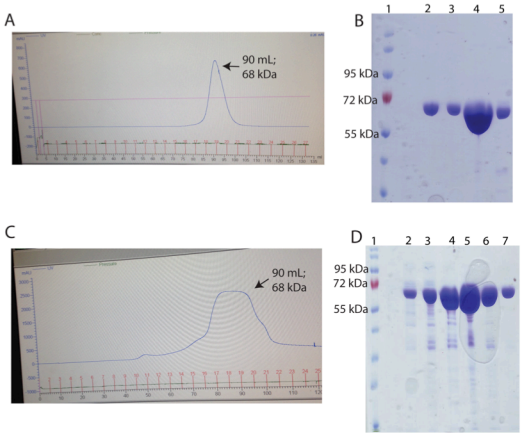

Fig. S13. Size exclusion chromatogram and SDS-PAGE gel analyses of MbnEs from *Mc. hirsuta* CSC1 (*A, B*) and *Mc. parvus* OBBP (*C, D*). Both MbnEs elute from the size-exclusion column as monomers (*A, C*) and have respective molecular weights of 66.7 and 68.03 kDa, observed in all fractions collected from the major peaks (*B, D*).

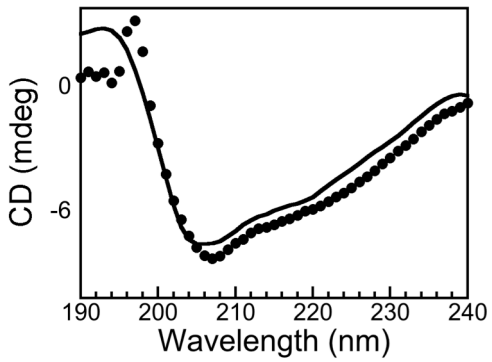

Fig. S14. CD spectrum and simulation thereof for the *Mc. hirsuta* CSC1 MbnE. Simulation parameters are reported in Table S8.

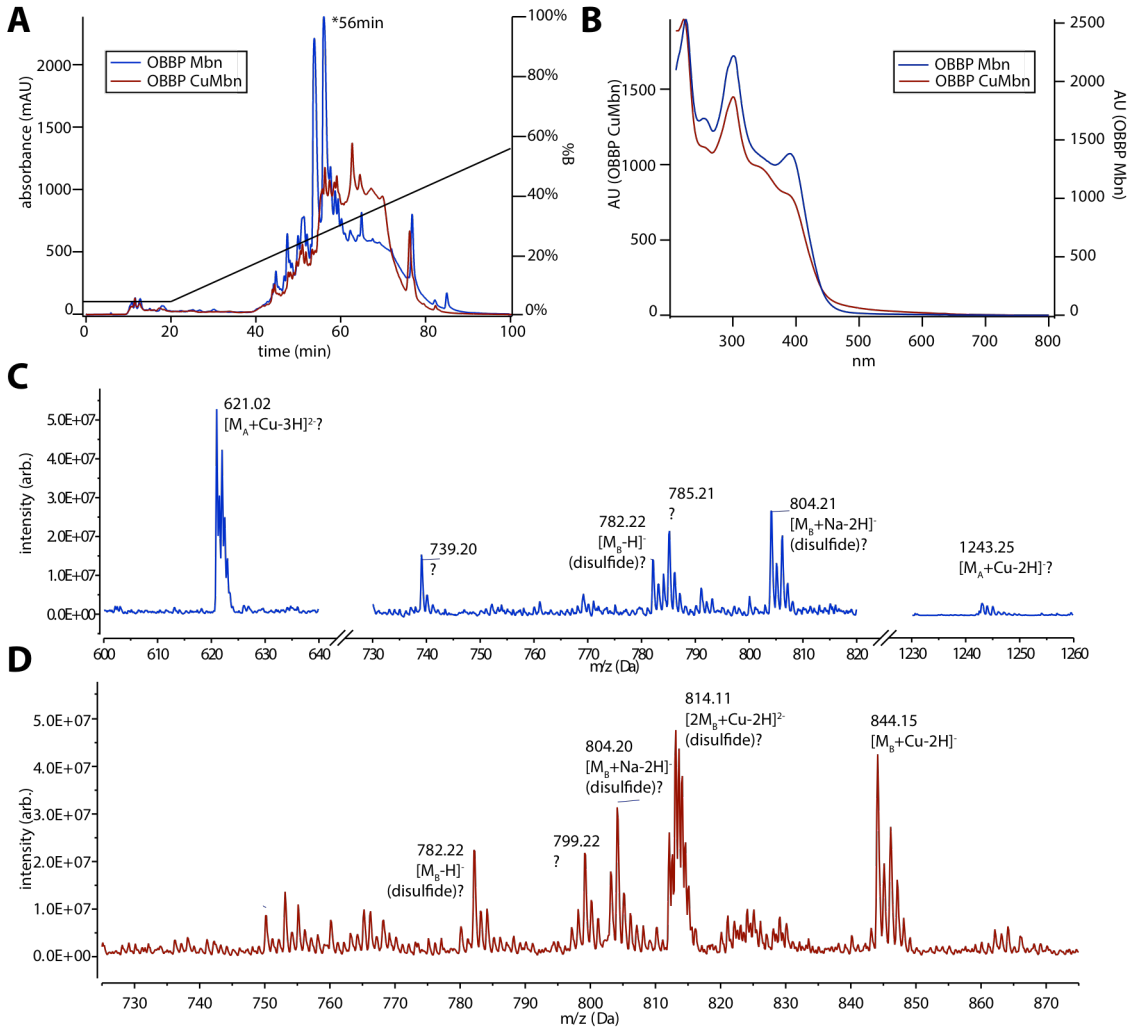

Fig. S15. Putative Mbns from *Mc. parvus* OBBP. (*A*) HPLC traces of apo (blue) and Cu (red) semi-purified *Mc. parvus* OBBP Mbn after Diaion elution and lyophilization. (*B)* UV-visible light spectra of the elution peaks at 56 min for apo (blue) and Cu (red) Mbn. The change in the 300-400 nm range is consistent with spectral changes that occur upon copper binding by other *Mc.* and *Ms.* species Mbns. (*C*) Mass spectrometry data for apo Mbn at 56 min support the presence of at least two major species, one a larger copper-binding species potentially consistent with a Group I Mbn missing C-terminal residues (M_A) and one a lower molecular weight species potentially consistent with a Group IIB Mbn (M_B). Several adducts and compounds of similar mass are observed in this region; it is not yet clear whether they are all derivatives of the same base compound affected by oxidation, disulfide formation, adduct formation, or other modifications. (*D*) Mass spectrometry data for Cu-exposed *Mc. parvus* OBBP Mbn at 56 min support copper binding by the low molecular weight species, in addition to copper-mediated dimer formation.

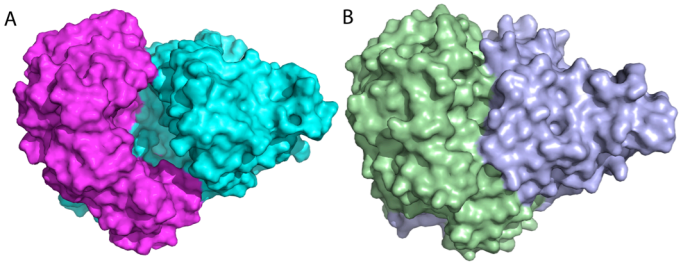

Fig. S16. Surface representation of crystal structures of *Mc. parvus* OBBP MbnE (5ICQ, *A*) and *Bacillus subtilis* AppA (1XOC, *B*). The nonapeptide co-crystallized with AppA is occluded from solvent due to substrate induced protein rearrangements.

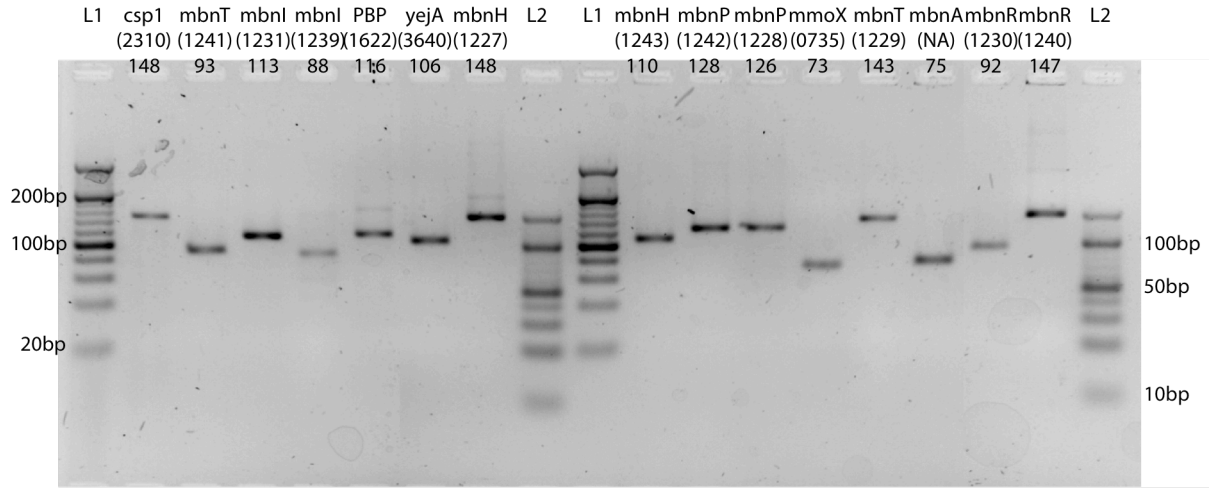

Fig. S17. qRT-PCR amplicons, visualized on a 4% NuSieve 3:1 gel in 1x TBE. Locus tags and predicted amplicon sizes are listed below the gene name.

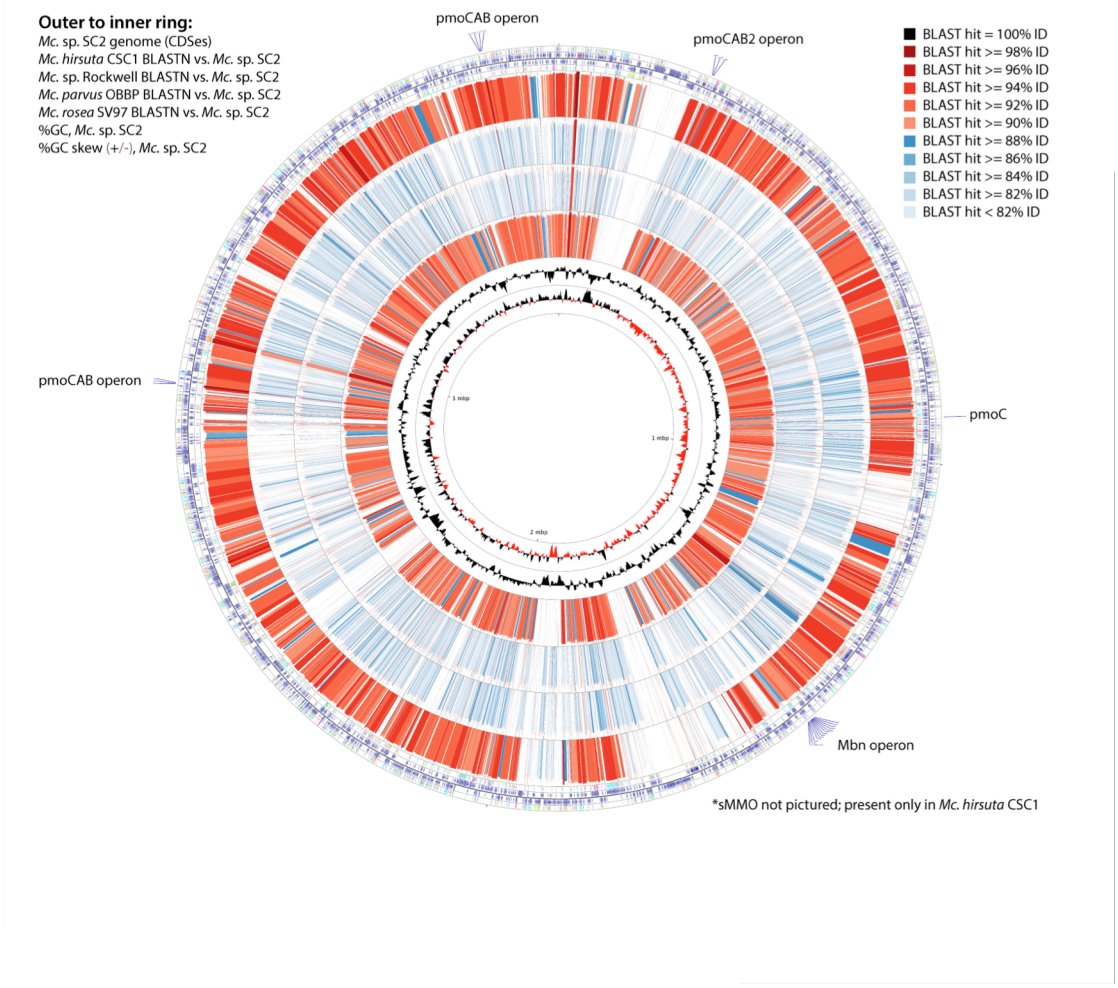

Fig. S18. Comparison of genomic sequences of other *Methylocystis* species against the genes present in the complete and closed genome of *Mc.* sp. SC2.

Supporting Tables

Table S1. Spearman correlation values between pairs of genes in the *mbn* operon and potentially co-regulated genes. Šidàk correction for multiple testing: p-value of 0.00233. Correlations with better p-values are highlighted in green; correlations with p-values worse than this but better than 0.05 are highlighted in yellow. Full list is available in SI File 5.

***mbn* operon vs. *mbn* operon (no *mbnIR*)**

target 1	target 2	ρ_s	p-value
mbnA	mbnT	0.965035	0.000000
mbnA	mbnP	0.972028	0.000000
mbnA	mbnE	0.923077	0.000000
mbnP	mbnE	0.874126	0.001433
mbnT	mbnP	0.930070	0.000000
mbnT	mbnE	0.951049	0.000000

***mbn* operon vs. non-*mbnE* PBPs**

target 1	target 2	ρ_s	p-value
mbnA	yejA	-0.006993	0.982461
mbnA	mbnE2	-0.335664	0.358039
mbnE2	mbnE	-0.272727	0.459932
mbnE2	mbnP	-0.223776	0.549566
mbnP	yejA	0.013986	0.971973
mbnT	mbnE2	-0.363636	0.320596
mbnT	yejA	-0.006993	0.982461
yejA	mbnE	0.020979	0.948978

***mbnI* vs. non-operon *mbnIR* homologues**

target 1	target 2	ρ_s	p-value
mbnI	mbnI3	0.755245	0.019571
mbnI	mbnR3	0.769231	0.015684
mbnI	mbnR2	0.615385	0.073319
mbnI2	mbnI	0.391608	0.269265

mbn* operon vs. non-operon *mbnTPH

target 1	target 2	ρ_s	p-value
mbnA	mbnH2	0.762238	0.017871
mbnA	mbnP3	0.727273	0.026864
mbnA	mbnT3	0.692308	0.037857
mbnA	mbnP2	0.601399	0.078302
mbnA	mbnH3	0.573427	0.097625
mbnA	mbnT2	0.566434	0.099434
mbnH2	mbnE	0.804196	0.010546
mbnH3	mbnE	0.678322	0.045297
mbnP	mbnH2	0.720280	0.030510
mbnP	mbnH3	0.496503	0.162708
mbnP	mbnT2	0.489510	0.164169
mbnP	mbnP2	0.489510	0.164169
mbnP2	mbnE	0.713287	0.031037
mbnP3	mbnE	0.776224	0.014198
mbnP3	mbnP	0.622378	0.070401
mbnT	mbnH2	0.783217	0.013310
mbnT	mbnP3	0.741259	0.022550
mbnT	mbnT3	0.706294	0.034338
mbnT	mbnH3	0.643357	0.058143
mbnT	mbnP2	0.643357	0.058143
mbnT	mbnT2	0.573427	0.097625
mbnT2	mbnE	0.587413	0.087693
mbnT3	mbnE	0.783217	0.013310
mbnT3	mbnP	0.573427	0.097625

Table S2. Crystallographic statistics for apo *Mc. parvus* OBBP MbnE	
Wavelength	1.0332 Å
Resolution	46 – 1.9 Å
Space group	$C222_1$
Cell dimensions	
a, b, c (Å)	122.2, 141.5, 83.1
Completeness (%)	100 (100)
R-factor, observed (%)	16.4 (72.5)
R-factor, expected (%)	16.6 (73.6)
I/σ	22.93 (5.68)
R-factor, measured (%)	17 (75.1)
CC½	99.9 (95)
R/R_{free}	0.164/0.198

Table S3. RNA quality control

	Concentrations (ng/μL)			RIN		
	1	2	3	1	2	3
0m	290	850	995	9.4	6.9	7.1
15m	310	1410	1350	9.2	7.4	7.4
5h	252	1135	635	8.4	9.9	7.8
24	315	1025	1235	9.3	9.4	6.9

Table S4. qRT-PCR primers

Target (Locus ID)	Forward	Reverse	Amplicon (bp)	Efficiency (%)
pmoB (MettrDRAFT_0382)	GGAATATATCCGCATGGTCGAG	GTAGACCATCATCGACACGAAG	103	94.0
pmoA (MettrDRAFT_0383)	GGAATATATCCGCATGGTCGAG	GAATACCACTTACCGACGAACC	135	88.3
mbnH homologue (MettrDRAFT_1227)	CGCGGGCATGATCTTTATTTC	CCTTTCCATCGATGTCGTAGAG	148	94.8
mbnP homologue (MettrDRAFT_1228)	GCCATTTCCTTTGCTCTGATG	CGCGAAGCCATGGACATA	128	97.3
mbnT homologue (MettrDRAFT_1229)	TTCCGCTCTACCTCTCCTATC	CATGTCCTGACCGTAAACTCC	143	102.5
mbnR homologue (MettrDRAFT_1230)	CGCGGCTATATCCTCTGC	CACGATCAGATAATCGGTGAGG	147	79.1
mbnI homologue (MettrDRAFT_1231)	AGGAGACATTGGCGCATAAG	CATCGGAATATCCTCGAAGACG	113	100.9
mbnI homologue (MettrDRAFT_1239)	TGGAGGCAATGGAGAAATGG	TTCATATAGAGCACGAACACCTC	88	101.5
mbnR homologue (MettrDRAFT_1240)	CGGCTGATCTTTGCGGATG	AGAGCGGGATCGAGGAAAG	92	99.9
mbnT homologue (MettrDRAFT_1241)	CACCAAAACCAATGTACCGC	AGATCAAACTCGAAGCCCTG	93	96.4
mbnP homologue (MettrDRAFT_1242)	GCCATTTCCTTCGCTCTGA	CGCGAAGCCATAGACATAGAG	113	99.1
mbnH homologue (MettrDRAFT_1243)	CGAAAGCAAAGATCCCATTTCC	CCTCGCCCTGCAGATAATG	110	107.9
PBP (MettrDRAFT_1622)	AGGGCTTCGTCTTCAATCTG	GTAGAGGCCGGAATAGAGATTG	116	94.8
secA (MettrDRAFT_1638)	CATGATCGAGAAGCAGGTGG	TCGGACTTGTATTCGTTGAGC	138	112.8
csp1 (MettrDRAFT_2310)	GCACCAATTCCGCTTTCAC	TTATGGCACTCTTCCGCAC	148	99.4

mmoR (MettrDRAFT_2359)	GCAAGGAGCATTTCAACCG	GATCTTGAGACAGCCGAGC	146	112.1
mmoX (MettrDRAFT_2362)	TTCAAAGAGAACCGGACGAAG	TGACCTTGAACTGCTCCTTG	73	92.5
ptsH (MettrDRAFT_2387)	ATCTCGTGATCTGCAACCG	GTCAGTATGCCCATGATCGAG	142	105.6
gcp (MettrDRAFT_2542)	CGGTTTGCGTTTCGTCATG	AAATCGAGGTCGTTGGTGAG	111	101.6
recA (MettrDRAFT_2640)	GTTGAAATTCTACGCTTCGGTG	ACCTTGTTCTTGACCACTTTGA	111	98.3
alaS (MettrDRAFT_2641)	TGATCCGACCTTGATGTTCAC	GTCGAGATCATTGTGCTTGC	139	103.2
mbnE (MettrDRAFT_3413)	GAGAGCCTCAATCGCTTCAA	CCATAATAGGTCTTCCGCTCATC	113	101.5
mbnI (MettrDRAFT_3419)	GCGTTCATCCTCTACGTTTCT	CTGAAGAGCGAGACGGATATG	105	99.8
mbnT (MettrDRAFT_3421)	GATCGGTTACGATTGGACCTTC	GTAAGTCGGTGTCATGAAGAGG	160	91.0
mbnA (NA)	TGACTGTCAAGATTGCTCAGAA G	GATAGCACGAACCGCAAAG	75	90.1
mbnP (MettrDRAFT_3426)	CTCTACGTCTATGGCTTCGAG	GCGTATTGCCAATCGTTCTG	83	89.2
glyA (MettrDRAFT_3587)	TGCTCACCAATGACGAAGAG	TTGCTGATAGGCCTTGAACTC	146	96.4
yejA (MettrDRAFT_3640)	AGCGTGTTCAAAGACCCG	AGGAGCTGGTGCGTTTATAAG	106	94.6
pssA (MettrDRAFT_4197)	GTCGCCTTCTACATCGTCTATG	CGAACAGGACCAGGATCAC	121	106.1

Table S5. List of primers used for the cloning of Δ*mbnT* mutant of *Ms. trichosporium* OB3b

DNA fragment	Forward primer (5' – 3')	Reverse primer (5' – 3')
mbnT 5' upstream region	TCACTCATTAGGCACCCCAGGCAT CATGGTCGGACCAGCGTGA	CATCGTTGCTGCTGCGTAACATCGCT CTACCTCGATCAGCCGC
gentamicin resistance gene replacing *mbnT*	ATGTTACGCAGCAGCAACGATGTT	TTAGGTGGCGGTACTTGGGTCG
mbnT 3' downstream region	CGACCCAAGTACCGCCACCTAAGA CGTTCGGGTCTTCTTCGCC	AAGTTGGGTAACGCCAGGGTTGCGCA GGAAACTCGGATGTGAG
mbnT sequencing	TCTATCCTTATTCATGGCGTAACGC	GATCGACGGATAATTCTCAAGATAGA

Table S6. List of primers used for the cloning of transport proteins

Protein	Forward primer (5' – 3')	Reverse primer (5' – 3')
Ms. trichosporium OB3b MbnT	GTCGACAAGCTTGCCGACTCGC CCGCAC	GTGGTGCTCGAGGAATTCCACG CGAATG
Mc. rosea SV97T MbnT	ACACGACCATGGCACAGCAGGC GCTTCCGC	TTCAGGCTCGAGAAACTTGAGT TTGATGCCTCCGG
Ms. trichosporium OB3b MbnE	TACTTCCAATCCATGTCTCAGGC GGCGGAGCC	TATCCACCTTTACTGTTATTTGC GCTGATCGAACCACCAATC
Mc. hirsuta CSC1 MbnE	ATGCAT CCATGG ATAAGTCTTTGAGCGCTCCCG	ATGCATGCGGCCGCACGGACG TCGGCTTTCTC
Mc. parvus OBBP MbnE	TACTTCCAATCCATGGGCCCGAT GAGCGATCCC	TATCCACCTTTACTGTTATGGA TTCTTTCTCCACCAGCTTTC

Table S7. CD spectrum deconvolution results for *Ms. trichosporium* OB3b MbnE

Structure	Protein fraction
α-helix, regular	0.282
α-helix, distorted	0.211
β-sheet, regular	0
β-sheet, distorted	0.037
Turns	0.114
Unordered	0.356

Table S8. CD spectrum deconvolution result for *Mc. hirstuta* CSC1 MbnE

Structure	Protein fraction
α-helix, regular	0.263
α-helix, distorted	0.227
β-sheet, regular	0.028
β-sheet, distorted	0
Turns	0.176
Unordered	0.31

Supporting Files

File S1. MbnT sequences, fasta
File S2. MbnT metadata, Excel
File S3. MbnT EFI-SSN, Cytoscape
File S4. MbnE EFI-SSN, Cytoscape
File S5. Excel sheet containing CNRQ data, full Spearman correlation values, and ANOVA table for qRT-PCR data
File S6. GenBank file of *Mc. hirsuta* CSC1 genome, annotated

References

1. Kenney GE & Rosenzweig AC (2013) Genome mining for methanobactins. *BMC Biol* 11(1):17-35.
2. Finn RD, Clements J, & Eddy SR (2011) HMMER web server: interactive sequence similarity searching. *Nucleic Acids Res* 39:W29 - W37.
3. Smith AT, Smith KP, & Rosenzweig AC (2014) Diversity of the metal-transporting P1B-type ATPases. *J Biol Inorg Chem* 19(6):947-960.
4. Cline MS*, et al.* (2007) Integration of biological networks and gene expression data using Cytoscape. *Nat Protoc* 2(10):2366-2382.
5. Wittkop T*, et al.* (2011) Comprehensive cluster analysis with Transitivity Clustering. *Nat Protoc* 6(3):285-295.
6. Gerlt JA*, et al.* (2015) Enzyme Function Initiative-Enzyme Similarity Tool (EFI-EST): A web tool for generating protein sequence similarity networks. *Biochim Biophys Acta* 1854(8):1019-1037.
7. Kenney GE, Sadek M, & Rosenzweig AC (2016) Copper-responsive gene expression in the methanotroph *Methylosinus trichosporium* OB3b. *Metallomics* In press(DOI: 10.1039/c5mt00289c).
8. Balasubramanian R, Kenney GE, & Rosenzweig AC (2011) Dual pathways for copper uptake by methanotrophic bacteria. *J Biol Chem* 286(43):37313-37319.
9. Galens K*, et al.* (2011) The IGS standard operating procedure for automated prokaryotic annotation. *Stand Genomic Sci* 4(2):244-251.
10. Stothard P & Wishart DS (2005) Circular genome visualization and exploration using CGView. *Bioinformatics* 21(4):537-539.
11. Studier FW (2005) Protein production by auto-induction in high density shaking cultures. *Protein Expr Purif* 41(1):207-234.
12. Provencher SW & Gloeckner J (1981) Estimation of globular protein secondary structure from circular dichroism. *Biochemistry* 20(1):33-37.
13. van Stokkum IHM, Spoelder HJW, Bloemendal M, van Grondelle R, & Groen FCA (1990) Estimation of protein secondary structure and error analysis from circular dichroism spectra. *Anal Biochem* 191(1):110-118.
14. Kabsch W (2010) XDS. *Acta Crystallogr D Biol Crystallogr* 66(2):125-132.
15. Kabsch W (2010) Integration, scaling, space-group assignment and post-refinement. *Acta Crystallogr D Biol Crystallogr* 66(2):133-144.
16. Long F, Vagin AA, Young P, & Murshudov GN (2008) BALBES: a molecular-replacement pipeline. *Acta Crystallogr D Biol Crystallogr* 64(1):125-132.
17. Adams PD*, et al.* (2010) PHENIX: a comprehensive Python-based system for macromolecular structure solution. *Acta Crystallogr D Biol Crystallogr* 66(2):213-221.
18. Emsley P & Cowtan K (2004) Coot: model-building tools for molecular graphics. *Acta Crystallogr D Biol Crystallogr* 60(Pt 12 Pt 1):2126-2132.
19. Winn MD*, et al.* (2011) Overview of the CCP4 suite and current developments. *Acta Crystallogr D Biol Crystallogr* 67(Pt 4):235-242.
20. Murshudov GN*, et al.* (2011) REFMAC5 for the refinement of macromolecular crystal structures. *Acta Crystallogr D Biol Crystallogr* 67(Pt 4):355-367.
21. Chen VB*, et al.* (2010) MolProbity: all-atom structure validation for macromolecular crystallography. *Acta Crystallogr D Biol Crystallogr* 66(Pt 1):12-21.

22. Schrodinger, LLC (2015) The PyMOL molecular graphics system, version 1.8.
23. Vita N*, et al.* (2015) A four-helix bundle stores copper for methane oxidation. *Nature* 525(7567):140-143.
24. El Ghazouani A*, et al.* (2012) Variations in methanobactin structure influences copper utilization by methane-oxidizing bacteria. *Proc Natl Acad Sci USA* 109(22):8400-8404.